CFD simulation and experimental analysis of cooling performance for thermoelectric cooler with liquid cooling heat sink

Burak Muratçobanoğlu[1] · Emre Mandev[1] · Mehmet Akif Ceviz[1] · Eyüphan Manay[1] · Faraz Afshari[1]

Abstract

Thermoelectric coolers are preferred in many areas because of their simple mechanism and no need for a refrigerant. In this study, an air-to-water mini thermoelectric cooler system was designed and produced. Experiments were performed by placing different numbers of thermoelectric modules on the liquid-cooling heat sink and applying different voltages. The cooling capacity and COP values of the system under different operating conditions were analyzed and discussed. In addition, the effect of fluid flow rate on system performance and temperature difference between inlet and outlet sections has been presented. The heat transfer and flow behavior of the fluid in the liquid-cooling heat sink were determined using CFD simulation methods. Moreover, the heat loss from the system was tried to be reduced by using extra foam insulation and the results were compared with single foam and the effect of the insulation on the temperature drop inside cooler was discussed. At 0.011 kg s^{-1} mass flow rate and 12 V voltage conditions, when the number of TE modules is increased from 1 to 3 in the TE cooler, a maximum increase of 35% in cooling load is obtained. Also, if the cases with 3 TE modules and 0.011 kg s^{-1} flow rate are compared in terms of cooling load, 12 V has 80% higher cooling load than 4 V. According to the numerical results, flow structures that negatively affect the heat transfer interactions and reduce the cooling performance of the TE cooler have been determined in the liquid-cooled heat exchanger. Additionally, a significant decrease in the temperature of the cooling chamber has also been achieved with additional insulation.

Abbreviations

COP	Coefficient of performance
CFD	Computational fluid dynamics
TE	Thermoelectric
P	Peltier

List of symbols

μ	Dynamic viscosity (kg m^{-1} s^{-1})
μ_t	Turbulent viscosity (kg m^{-1} s^{-1})
$\forall$	Volume (m^3)
C_μ	Turbulence constant
C_p	Specific heat capacity (J kg^{-1} K^{-1})
G_k	Generation of turbulent kinetic energy
I	Electric current (A)
k	Thermal conductivity (W m^{-1} K^{-1})
m	Mass (kg)
Q_c	Cooling load (J)
T	Temperature (°C)
t	Time (s)
V	Voltage (V)
v	Velocity (m s^{-1})
W	Power consumption (W)
ϵ	Turbulent dissipation rate (m^2 s^{-3})
ρ	Density (kg m^{-1})

Subscripts

a	Air
f	Final
i	Initial

✉ Emre Mandev
emre.mandev@erzurum.edu.tr

Burak Muratçobanoğlu
burak.muratcobanoglu@erzurum.edu.tr

Mehmet Akif Ceviz
akif.ceviz@erzurum.edu.tr

Eyüphan Manay
emanay@erzurum.edu.tr

Faraz Afshari
faraz.afshari@erzurum.edu.tr

1 Department of Mechanical Engineering, Erzurum Technical University, Erzurum, Turkey

Introduction

Thermoelectric (TE) cooling method is widely used due to its advantages such as no refrigerant, no need to mechanical devices, and easy temperature control. Although thermoelectric cooling has low efficiency and high cost, it is preferred more in small size and portable coolers than vapor compression cooling, which has a more compact structure. Thermoelectric cooling occurs when a direct current is applied to an interface, transferring thermal energy by electrons and thus creating a temperature difference between the two surfaces. Jean Peltier discovered this principle in 1834, and this effect is described by his name. Moreover, the thermoelectric effect, which provides the conversion of electrical and thermal energy, consists of *P*-type and *N*-type semiconductors connected electrically in series and thermally in parallel [1–5].

Thermoelectric cooling is used in many fields, including the condensation of moisture in the air [6], cooling of electronic equipment (such as microprocessors) [7–10], battery thermal management systems of electric vehicles [11, 12], air cooling systems [13, 14], reducing the temperature of solar panels or heat exchangers [15–18], air conditioning systems for vehicles [19–21] and cooling systems (such as refrigerators) [22–24]. Thermoelectric coolers have some advantages comparison conventional vapor compression coolers. Silence, easy temperature control, and not having a complex structure are some of these advantages. For this reason, many researchers have carried out various studies on thermoelectric coolers and tried determining the optimum working conditions [25].

The efficient usage of thermoelectric coolers depends on the effective removal of the heat absorbed by the thermoelectric module from the system. Researchers have applied various methods to remove waste heat. The most common of these methods are natural convection through various heat sinks, forced convection using devices such as fans, and the transfer of heat to the flowing liquid from a heat exchanger such as a mini-channel. In a study examining the removal of waste heat from the TE cooler by natural convection, the effect of the radiation heat transfer effect on the COP value of the system was demonstrated. This study was determined that the COP value of the TE cooler increases significantly when the radiative heat transfer was taken seriously [26]. Baldry et al. [27] designed a heat sink that provides the heat to be removed with natural convection from the hot side of the thermoelectric module. The thermal resistance of this heat sink is quite low. Numerical and experimental analyses performed have shown that the heat is removed quite well by this designed heat sink. In another study, an experimental and numerical optimization was made on the TE cooler designed and manufactured. In this study, 6 TE modules were used and 9 different situations were examined according to the positions of these TE modules. Heat sinks were placed in the cold side and the hot side of the TE modules. By means of these heat sinks, natural convection conditions in the interior of the chamber and forced convection conditions with fans in the exterior were applied. Optimal arrangement was reached when all TE modules were at the top of the chamber [28]. Another study carried out to determine the optimum operating conditions of the TE cooler was a heat sink and fan placed on both surfaces of the TE module. The effect of the voltage applied to the TE module and fans was investigated. Comparisons were made in the inside of the cooler under natural convection and forced convection conditions. The optimal operating voltages for this study are reported to be in the range of 10–11 V for the TE module, 4–6 V for the fan on the cold side, and 10 V for the fan on the hot side [29]. In a study carried out to determine the optimum operating voltages of the TE cooler, experiments were performed under forced convection conditions by placing fans on both sides of the TE module. Observations were made at different voltage values applied to the both fans and the TE module and it

Table 1 Literature summary on COP values of TE coolers

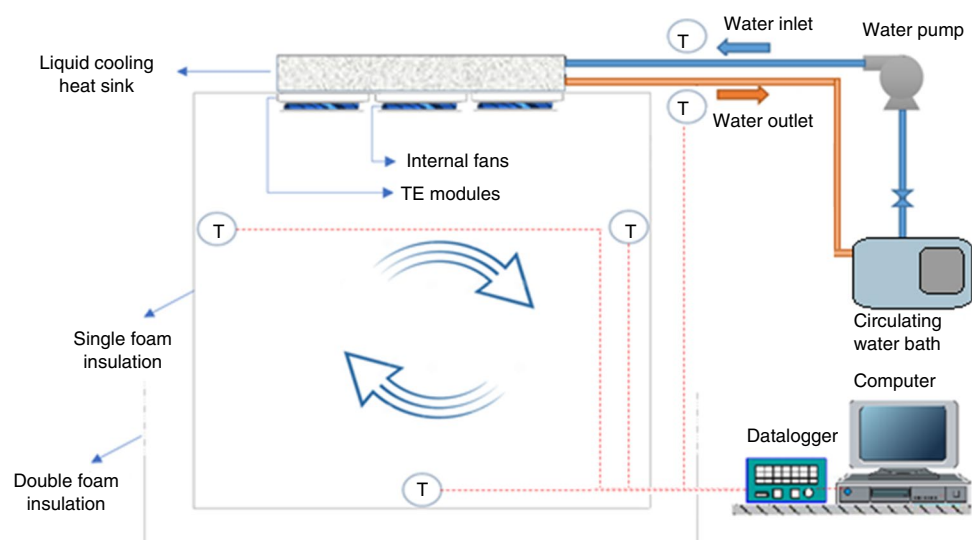| References	Volume of chamber	Heat removal method	ΔT $(T_{amb} - T_i)$	COP
Vian and Astrain [40]	0.225 m³	Capillary lift thermosyphon	19 °C	0.45
Min and Rowe [41]	40 L	Liquid circulation	10 °C	~0.3
Rahman et al. [42]	6.5 cm×6.5 cm×15 cm	Finned heat exchanger and fans	–	0.61
Abderezzak et al. [43]	0.0216 m³	Finned heat pipes and fan	13 °C	0.297
Mirmanto et al. [44]	215 mm×175 mm×130 mm	Finned heat sink and fan	–	<0.03
Ohara et al. [45]	10 cm×12 cm×9 cm	Finned heat sink and fan	17.6 °C	~0.3
Jugsujinda et al. [46]	25 cm×25 cm×35 cm	Finned heat exchanger and fan	–	0.65
Tamami et al. [47]	–	Water block, finned heat sink and fan	14.9 °C	0.3
Hermes and Barbosa [48]	56 L	Heat spreader and fan	19.8 °C	~0.2

was reported that the optimum voltage values for the inner fan, outer fan and TE module were 3 V, 9 V and 12 V, respectively [30]. A thermosiphon phase change material was developed by Vian and Astrain [31] to improve the performance of the TE cooling system. The finned heat exchanger with natural convection was compared with this developed system and it was detected that the system increased the COP value by 32%. In a study conducted to determine the optimum voltage value applied to the TE module, observations were made on the internal chamber cooling and COP values by using 4 different voltage values (5, 10, 15 and 20 V). In this study, the authors showed the effect of the applied voltage on the cooling performance, but they emphasized that the increased voltage decreased the COP value [32]. In a study by Martinez et al. [33] was reported that the electricity consumption of the TE cooler was reduced with the temperature controller. The effects of the thermal resistance of the heat sinks and the voltage applied on the performance and COP value of the TE module were investigated. It has been shown that the COP value decreases as the thermal resistance increases [34]. In a study to improve the performance of the TE cooler, PCM was added and compared to the system with conventional heat exchangers on both surfaces of the TE module. This change provided significant increases in the performance of the system, and thus, it was reported by authors that the temperature increase could be prevented in cases such as opening chamber door [35].

It is known that the heat transfer performance of liquids is better than gases. Therefore, researchers have designed TE coolers that transfer heat from air to water. Thus, the heat drawn from the cooling chamber is removed quicker from the system. In a study comparing the cooling performance and COP values of the TE cooler using air-to-air and air-to-water modes, it was observed that the COP values were approximately 30–50% higher in the air-to-water mode [36]. An eco-friendly TE cooler has been developed to keep fruits and vegetables cold. In this cooler, a liquid block is integrated on the hot side of the TE module and the heat in the system is transferred to the water. The cooling performance and COP value of the installed system were observed for 360 min and it was reported that the temperature of the cooling chamber decreased by 26.3 °C at the end of this period [37]. In another study, a liquid-cooled block is placed on the hot surface of the TE module, and a water-to-air heat exchanger is integrated into the system to cool the fluid with increasing temperature. In this study, 3 different water-based nanofluids (Al_2O_3, TiO_2 and SiO_2) were used and the effects of these fluids on the temperature drop and COP of the system were evaluated. For all nanofluids, the difference between the initial and final temperature of the system was higher than pure water. Al_2O_3-pure water nanofluid showed the highest effect [38]. The effect of the fluid flow rate on the COP value and cooling performance of the system was investigated in a study, in which the liquid-cooled method was used to remove the waste heat from the system. It has been reported that as the fluid flow rate increases, the

Table 2 Experiments plan sequence

	A	B	C	D	E	F	G	H	I
TE voltage	4 V	4 V	4 V	8 V	8 V	8 V	12 V	12 V	12 V
Mass flow rates	0.005	0.008	0.011	0.005	0.008	0.011	0.005	0.008	0.011

Fig. 1 Schematic view of the TE cooling system

internal temperature of the TE cooler decreases [39]. Additionally, a summary table containing chamber volumes, heat removal method, temperature difference and COP values for experimental studies on thermoelectric coolers is presented in Table 1.

As summarized above, when the studies in this field are examined, there is not enough information about the effect of the cooling water flow rate on the system performance and temperature change. In addition, there is no analysis on the effect of thermal losses caused by the TE system placed in the cooling chamber and the related heat sink applications. In this innovative study, comprehensive experimental and numerical analyses were conducted to investigate the impacts of cooling water flow rates and thermal losses on the cooling capacity and COP values of Thermoelectric systems across diverse operational scenarios. This study, not only sheds light on the operational principles and utilization scenarios of TE systems, which are rapidly gaining prominence, but also introduces novel insights into their performance. The obtained results are expected to make a significant and valuable addition to the existing body of knowledge in the field of thermoelectric cooling systems.

Experimental procedure

In this study, a cooling chamber with a capacity of 0.0031 m^3 made of Styrofoam was designed and produced to evaluate the Thermoelectric cooling performance under different voltages, coolant mass flow rates, and Peltier numbers. Experiments were carried out on an air-to-water TE cooling system using a heat sink, which is a water-cooled heat exchanger connected to the hot side of the TE. With the aim of improving the heat flow rate, thermal grease HY510 was used between the connected surfaces. As the main elements of the cooling system TEC1-12715 Peltier modules were selected and used. The dimensions of the TEs are 40 × 40 × 4 mm, which are operated at different voltages in the range of 4, 8 and 12 V. The Peltier modules were powered by the KXN-3020 brand power supply, with a sensitivity of 0.01 A and 0.1 V. SKU 50200 model a mini water pump device was used to circulate heat transfer fluid which

is pure water. Temperature values were measured using five T-type thermocouples with 0.05 °C sensitivity. In addition, Hioki LR8402-20 model data logger was used, which transfers the obtained data to the computer. The resolution of this used data logger is 0.01 °C.

The water flow rates of 0.005, 0.008, and 0.011 kg s^{-1} were considered which was provided using the mini water pump in the cycle. The water heated by TE, paths through a water tank equipped with a temperature regulation system (water bath). In the experiments, the water temperature of the water bath was adjusted to 20 °C. A TESTO 885-2 model thermal camera was used to take images of the cooling chamber in the single and double foam insulation modes. The measuring interval of the used thermal imager is between −30 °C and +350 °C, with accuracy and thermal sensitivity of ±2 °C and <30 mK, respectively. Three thermocouples have been used to measure the temperature variation inside the cooling box and two
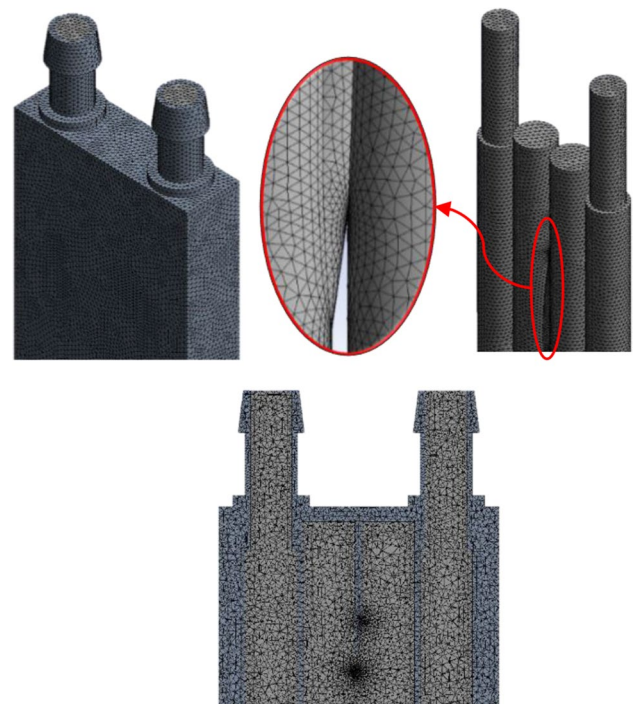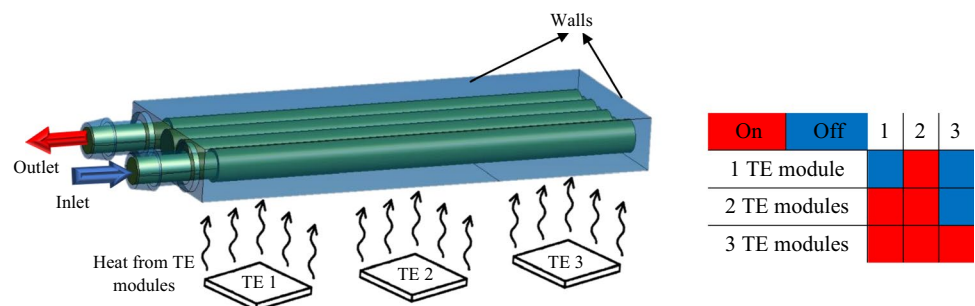

Fig. 3 Mesh configuration of liquid-cooling heat sink

Fig. 2 The geometry of liquid-cooling heat sink, boundary conditions and operating modes of TE modules

thermocouples were used to measure water inlet and outlet temperatures in the liquid-cooling heat sink over the test time. Voltage and current values have been recorded to calculate the consumed power of the cooling system. The experiments plane and naming is given in Table 2. Moreover, a schematic diagram of the entire cooling system is presented in Fig. 1.

The calculation procedure started with the calculation of the air mass in the cooling chamber. Here, the air mass m_a in the chamber is calculated by multiplying the volume of the cooling chamber and the density of the air, as given in Eq. 1.

$$m_a = \forall \times \rho \tag{1}$$

The electricity consumption of the TE module was obtained as shown in Eq. 2 by multiplying the current and voltage read from the power supply.

$$W = I \times V \times t \tag{2}$$

Afterward, the cooling load of the TE cooler was obtained as given as follows:

$$Q_c = m_a \times C_p \times (T_i - T_f) \tag{3}$$

Using Eqs. 2 and 3, the COP value of the system was calculated as given in Eq. 4.

$$COP = Q_c / W \tag{4}$$

Numerical approach

Computer-aided numerical studies visualize the experiment system in heat transfer and flow applications, thus providing the opportunity to analyze many important parameters such as flow characteristics and temperature distribution. Due to this mentioned contribution of numerical solutions, a numerical simulation has been made on the block where the flow and heat transfer is carried out in this study. All steps of the numerical simulation, such as creating the geometry of the block, generating the mesh, performing the analysis, obtaining the contours and results, were carried out using the ANSYS-Fluent database.

In the simulation, steady-state conditions were considered, radiative heat transfer was neglected and it was also assumed that the thermophysical properties of water do not change with temperature. Parallel solver was selected in Fluent launcher settings. Solver type and velocity formulation were chosen pressure-based and absolute, respectively. k-epsilon was chosen as viscous model and standard was also preferred as k-epsilon model. In the scheme section of the solution method, couple was chosen to give a more precise result. Second-order equations were used for pressure in the analysis. Moreover, momentum and energy equations were arranged as second-order upwind and turbulent kinetic

energy and turbulent dissipation rate as first-order upwind. In addition to all these, Reynolds-Averaged Navier–Stokes (RANS) equations were preferred because direct numerical simulation (DNS) is generally insufficient to simulate flow fields and vortexes.

Geometry and boundary conditions

The geometry of the heat sink has been created in the same dimensions as the dimensions specified in the experimental procedure details section. This geometry is presented in Fig. 2. Constant heat flux boundary conditions were applied to the regions where the TE modules were placed on the heat sink. The constant heat fluxes were calculated by multiplying the experimental current and voltage values applied to the module. In addition, the same values with the data obtained in experiments were used as the inlet mass flow and water temperature. In Fig. 2, the heat flux applied areas have been shown according to the number of TE modules used. The block material and fluid were chosen as aluminum and water, which are found in the Fluent database, respectively.

Mesh generation

In mesh generation, default settings were preferred and no method was applied. The skewness and element quality values were at the desired values eliminated the need to
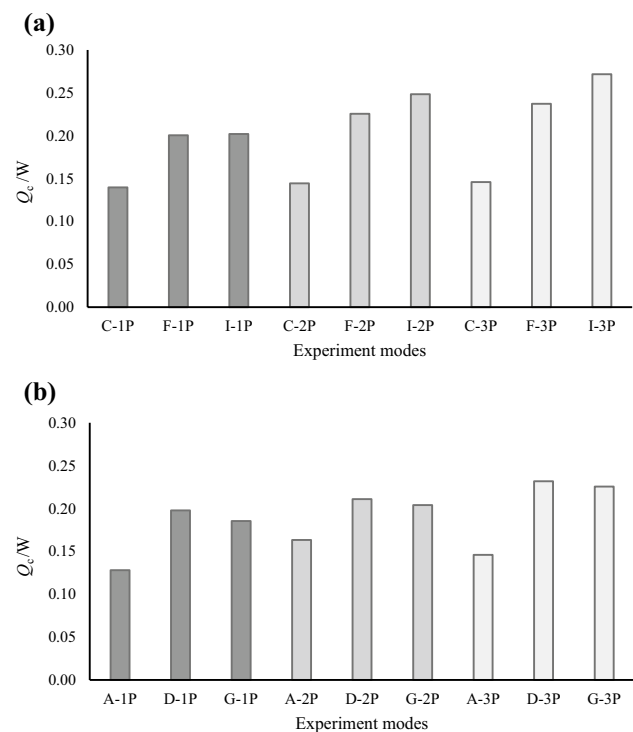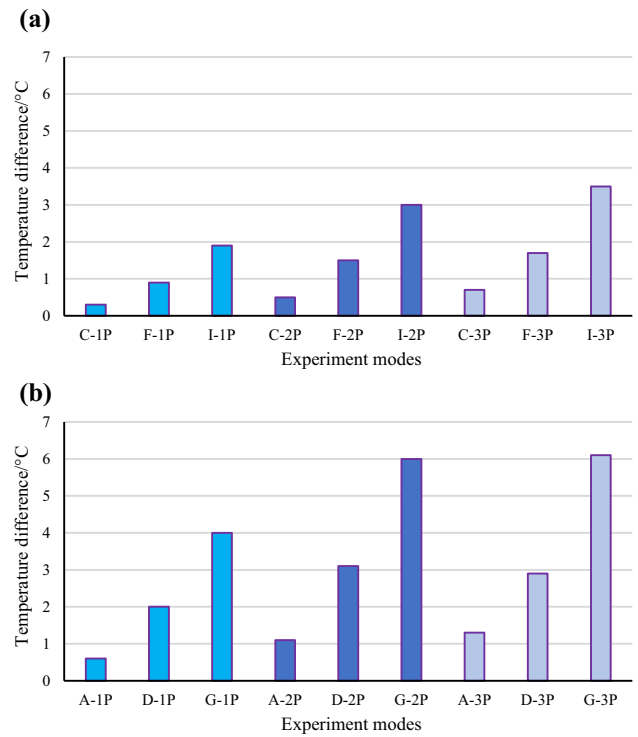

Fig. 4 Q_c variations with Peltier number and applied voltage at 0.011 kg s^{-1} flow rate (**a**) and at 0.005 kg s^{-1} flow rate (**b**) (single foam)
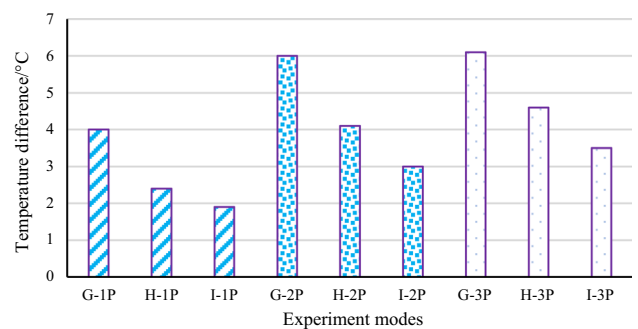
(a)

(b)
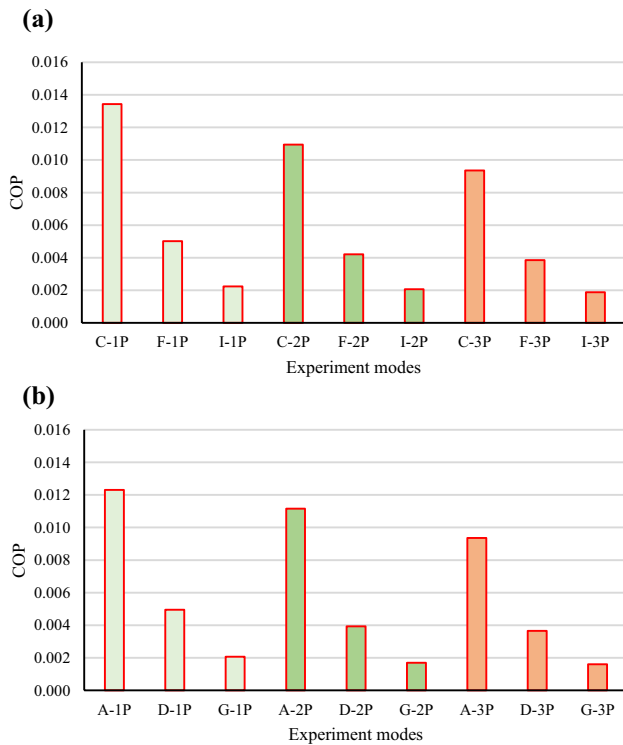
Fig. 5 COP variations with Peltier number and applied voltage at 0.011 kg s^{-1} flow rate (**a**) and at 0.005 kg s^{-1} flow rate (**b**) (single foam)

(a)

(b)

Fig. 6 Temperature difference between water inlet and outlet with Peltier number and applied voltage at 0.011 kg s^{-1} flow rate (**a**) and at 0.005 kg s^{-1} flow rate (**b**) (single foam)

use the method. In this study, only the element size has been changed and the mesh number has been brought to the desired number. It was seen that 950,000 was sufficient because the same results were obtained in more mesh numbers and all analyses were performed in this mesh number. In addition, the number of nodes was obtained as 196,883 under these conditions. The transition ratio, maximum layers and growth rate were set to 0.272, 5 and 1.2, respectively. Skewness values are values that show how well the created mesh size agrees to the optimum mesh size and is crucial for mesh quality. Therefore, a better-quality mesh is obtained with the smaller average skewness value. Skewness values in the range of 0–0.25 are considered excellent [49]. The average skewness value, standard deviation of the skewness and element quality obtained in this study are 0.23, 0.12 and 0.835, respectively. In Fig. 3, the mesh configuration of the fluid and solid is presented. In addition, the mesh structures in the interior are shown by taking a section from the middle of the geometry.
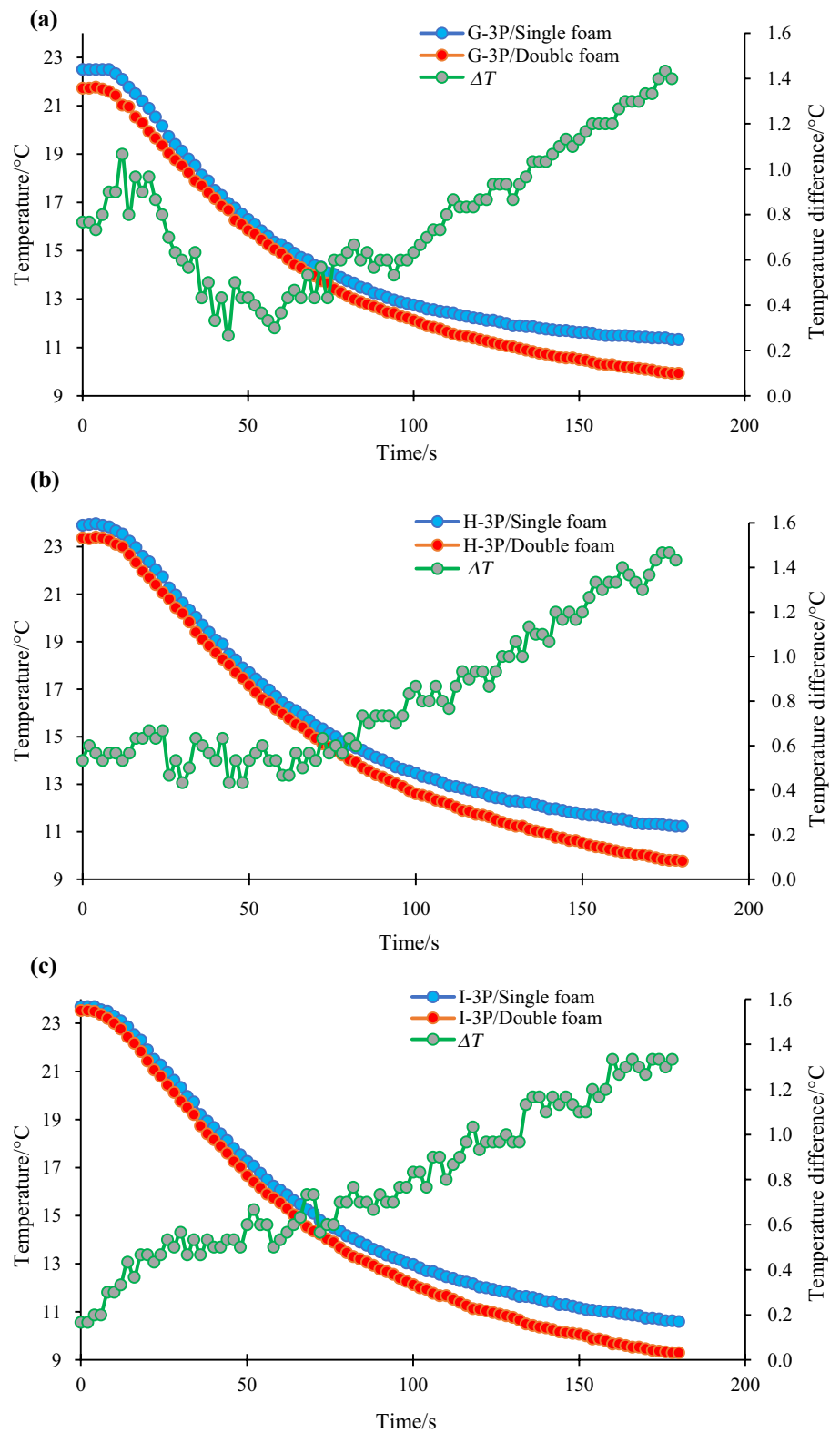

Fig. 7 Temperature difference between water inlet and outlet with flow rate and Peltier number at constant voltage (single foam)

Governing equations

There are three governing equations in the numerical solution of flow problems. These equations are momentum Eq. 5, energy conservation Eq. 6 and continuity Eq. 7, as presented below [50].

$$\nabla \cdot \left(\rho \cdot \vec{v} \cdot \vec{v} \right) = -\nabla p + \nabla \cdot \left(\mu \left[\left(\nabla \vec{v} + \nabla \vec{v}^T \right) - \frac{2}{3} \nabla \cdot \vec{v} I \right] \right)$$
(5)

Fig. 8 Comparison of single and double foam insulations effects on temperature drop at constant voltage and different flow rates

$$\nabla \cdot \left(\vec{V}(\rho E + p) \right) = \nabla \cdot k_{\text{eff}} \nabla T - h\vec{J}$$
$$+ \left(\mu \left[(\nabla \vec{v} + \nabla \vec{v}^T) - \frac{2}{3} \nabla \cdot \vec{v} I \right] \cdot \vec{v} \right) \tag{6}$$
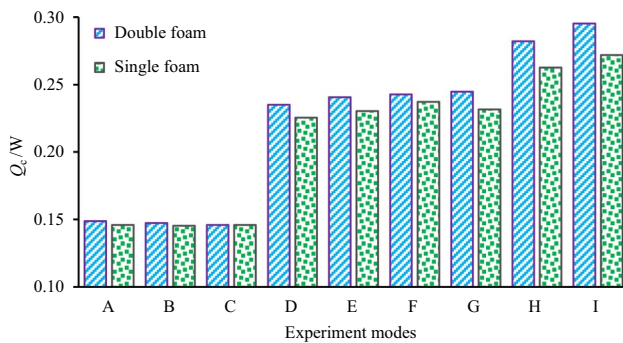
$$\nabla \cdot \left(\rho \cdot \vec{v} \right) = 0 \tag{7}$$

The *k*-epsilon turbulence model is widely used and recommended in CFD studies in the literature [51, 52]. The *k*-epsilon turbulence model provides two basic formulas for the flow field, defined as kinetic energy and the rate of dissipation of kinetic energy. These formulas have been presented as follows:

$$\frac{\partial}{\partial x_i} \left(\left(\frac{\mu_t}{\sigma_k} + \mu \right) \frac{\partial k}{\partial x_j} \right) - \rho \varepsilon + G_k = \frac{\partial}{\partial x_i} \left[(u_i \rho k) \right] \tag{8}$$
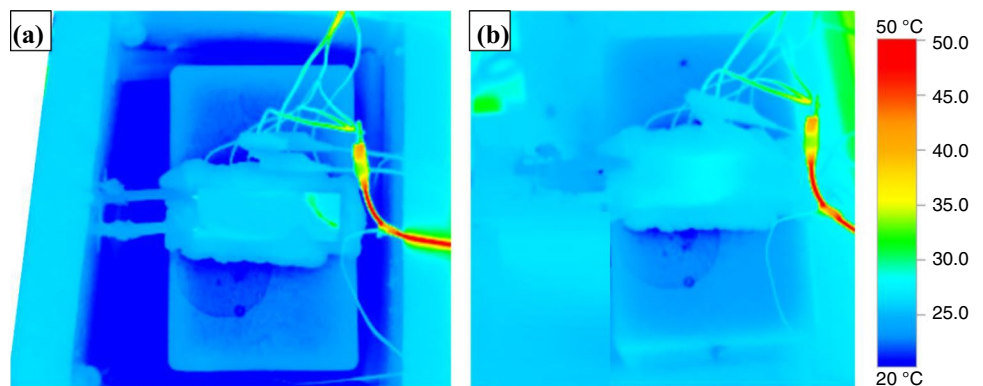
$$G_k = -\frac{\partial u_j}{\partial x_i} \rho \overline{u'_j u'_i} \tag{9}$$

$$\frac{\partial}{\partial x_i} \left(u_i \rho \varepsilon \right) = \frac{\partial}{\partial x_j} \left[\left(\frac{\mu_t}{\sigma_\varepsilon} + \mu \right) \frac{\partial \varepsilon}{\partial x_j} \right] + \frac{\varepsilon}{k} G_k C_{1\varepsilon} - \rho \frac{\varepsilon^2}{k} C_{2\varepsilon} \tag{10}$$

Fig. 9 Comparison of single and double foam insulations effects on Q_c for the case of 3 TE modules

The turbulent viscosity found in the equations presented can be obtained by the following equation [53];

$$\mu_t = \rho C_\mu \frac{k^2}{\varepsilon} \tag{11}$$

Result and discussion

In this section, the results of experiments and numerical analysis carried out under different conditions are presented and discussed as diagrams and visuals. Firstly, experimental evaluations were made and numerical results are given in the next subtitle.

Experimental results

In Fig. 4a, the average Q_c variations with the voltage applied and the number of TE at a fluid flow rate of 0.011 kg s^{-1} are given. It is seen that at a low flow rate of 0.005 kg s^{-1}, Q_c value increases as the Peltier number increases. By considering I cases, the Q_c value of the 3 TE is 35% higher than that of 1 TE case mode. If the cases of 3 TE modules are compared according to the amount of applied voltage, it can be seen that in the case of 12 V, the value of Q_c is about 80% higher than that of 4 V. On the other hand, when the flow rate increases, the heat of the TE is efficiently withdrawn and the Q_c value increases with the voltage and Peltier number as expected. In Fig. 4b, the average Q_c change with the different voltage applied to the TE module at 0.005 kg s^{-1} fluid flow rate and the number of TEs is given. The highest Q_c values were reached in the case of 3 TE modules and 8 V voltage. For the all cases, namely 1, 2 and 3 TE modules where 12 V voltage was applied, the heat transfer fluid could not absorb enough heat from the hot surface of the TE module and consequently Q_c value was lower than the case of 8 V.

The histograms in Fig. 5 present the average COP values of the system for both high and low flow rates. These

Fig. 10 Thermal camera images for double foam (**a**) and single foam (**b**) insulation modes
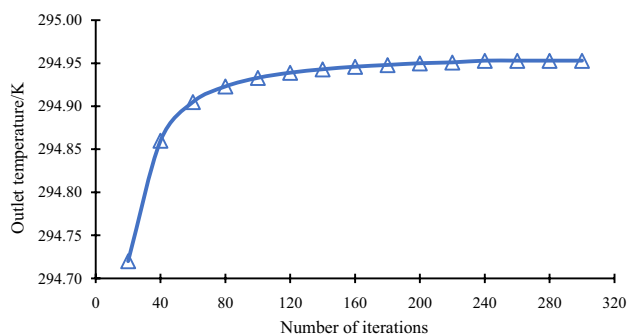
Fig. 11 Iterations analyses
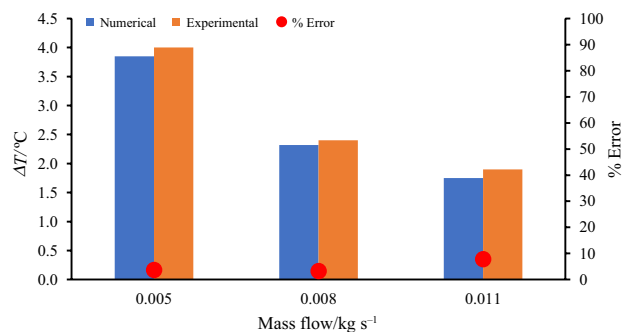
Fig. 12 The difference between the inlet and outlet temperatures of the water into the block and comparison of experimental and numerical data

values are displayed in relation to the Peltier number and voltage settings. It is crucial to explain the observed trends in the results. From the obtained results, with an increase in the Peltier number, the COP value exhibited a decrease, primarily attributable to the heightened electrical power consumption. In the installed experimental setup, elevating the applied voltage correspondingly resulted in an increase in electrical power consumption, thus exerting a detrimental impact on the COP. Even though the applied voltage remains constant for each Peltier number setting, the corresponding increase in current, correlated with higher Peltier numbers, amplifies the overall electrical energy consumption.

The water inlet and outlet temperature differences for the liquid-cooling heat sink are given in Fig. 6. Two different diagrams have been prepared for high and low water flow rates. When the two diagrams (Figs. 6a, b) are compared, the difference between the inlet and outlet temperatures is less at high flow rates, as expected. As the applied voltage and Peltier number increase, higher heat transfer occurs and as a result, the temperature difference of the water becomes evident. In Fig. 6b, the highest difference appeared between the A-1P (4 V) and G-3P (12 V) test modes, with an increase of approximately 10 times.

Figure 7 presents the effect of different flow rates in triple block heat exchanger and the number of TE modules on the temperature difference for 12 V supply voltage. Here, it is seen that the increasing number of TE modules significantly increases the temperature difference for all flow rates. This is due to the higher amount of heat transfer by multiple TE modules.

In addition, since the increase in the water flow rate increased the cooling efficiency, a significant decrease was observed in the temperature difference. The lowest temperature difference was obtained for the highest flow rate and 1 TE condition, as expected.

In Figs. 8a, b and c, the time variation of the cooling chamber temperatures for the cases G, I and H is presented, respectively. The experiments were repeated with insulation improvement using double foam insulation and the graphics including single foam and double foam situations have been presented. As the flow rate increased, cooling became more effective. This is because effective cooling of the hot surfaces of the TE modules was ensured, which in turn led to a decrease in the internal temperature of the cooling chamber. Additionally, it was observed that the flow rate had little effect on the temperature difference between single and double foam. A temperature difference of approximately 1.4 °C was obtained at all flow rates. In the presented diagrams, due to the increase in heat loss, the temperature difference between single and double foam applications increases over time, which shows the importance of insulation in low-temperature coolers.

As the test time passes, the difference between the chamber temperature and the ambient temperature increases for both cases, and this causes an increase in heat loss. However, the increase in the case of single foam is relatively higher than that of double foam. Additionally, at the lowest flow rate and with single foam (in the G case), initial cooling occurred more rapidly, which caused it to approach the internal temperature values of double foam. However, later on, due to higher heat losses to the surroundings, the temperature difference increased rapidly.

In Fig. 9, cooling loads for single foam and double foam insulation are compared for all flow rates and supply voltage values in 3 TE modes. When the figure is examined, in experiment modes A, B, and C, the results for double foam and single foam appear closely aligned and similar. However, as we progress to the subsequent modes, specifically D, E, F, G, H, and I, it becomes evident that double foam experiments provided significantly higher cooling loads than that of single foam experiments. In other words, the double foam effect becomes more pronounced with increasing supply voltage. This is due to the decrease in cooling chamber temperatures with increasing supply voltage. The highest improvement in Q_c was obtained in mode I with 11% difference by using double foam application.

Fig. 13 Velocity contours and streamlines of water in the heat sink at different mass flow rates

0.005 kg s^{-1} 0.008 kg s^{-1} 0.011 kg s^{-1}
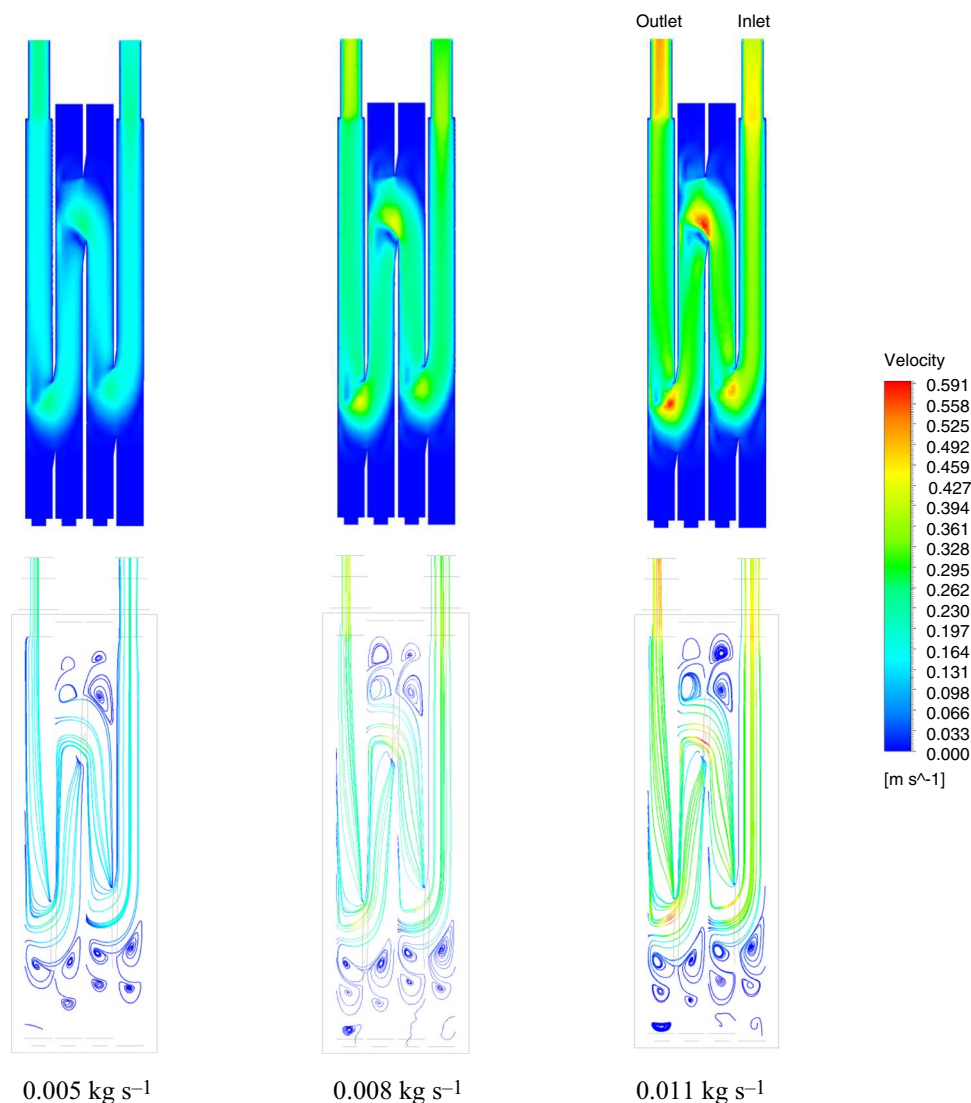
In Figs. 10a, b, thermal camera images are given for the cooling chamber where double foam and single foam insulations have been used, respectively. Considering Fig. 10a, low-temperature air mass is clearly seen between the two insulation layers. This means that the cooled air closes the first foam layer and is trapped, and heat loss to the environment due to natural convection is prevented. This situation increases the COP value of the system and causes a more effective cooling. However, the cooling chamber walls (first foam layer) in Fig. 10b are at ambient temperature, as expected. In addition, when the images are examined, a significant temperature rise (heat generation) is seen in the electrical cables connected to the system elements. Since this situation will adversely affect the performance of the system, it is recommended to eliminate this negativity by taking various cabling precautions in the ongoing studies.

Numerical results

In this section, the results obtained from the CFD solution are presented in the form of contours and diagrams. The thermal behavior of the liquid-Cooling Heat Sink and fluid under different operating conditions is visualized. Thanks to the results obtained, the experimental outputs and numerical results are compared. Moreover, all images were obtained using CFD post.

Obtaining correct results from the analyses made depends on the number of iterations. For this reason, in this study, iteration analysis has been performed to determine the optimum number of iterations. The analysis results are presented in Fig. 11. As can be seen from the figure, the same results are obtained for all iteration numbers after 240 iterations. Based on these results, all analyses have been carried out at 240 iterations.

**Fig. 14** Temperature contours of the water for the cases with 1 TE module
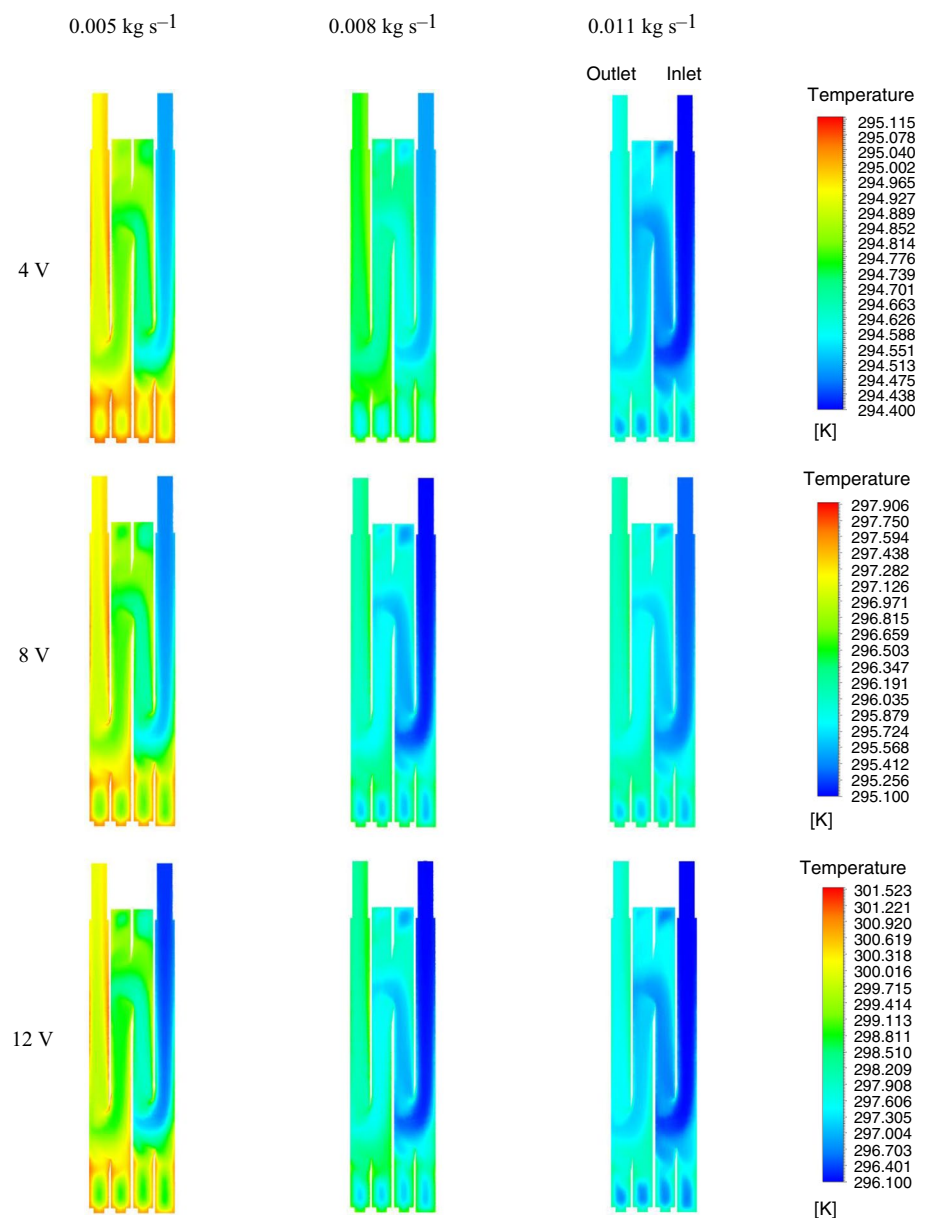
It is important that they match each other in experimental and numerical studies together. In order to get the reliable numerical solutions, large numerical analyses need to be validated with several experimental groups. For this reason, the outputs of the numerical and experimental work carried out under the same conditions are presented. In Fig. 12, results are given for the case where 12 V voltage is applied on 1 TE module. The difference between the inlet and outlet temperatures of the water in the block is presented at different mass flow rates. Also percentage (%) errors are shown in the diagram. As can be seen in the diagram, there is a strong agreement between the experimental and numerical data. The highest error rate is seen around 7.8% at 0.011 kg s^{-1}

flow rate. In other flow rates, this rate is a very small amount, such as 3%.

In Fig. 13, the velocity distributions and streamlines of the fluid circulating in the heat sink are given at different mass flow rates. In the connection regions between channels, the fluid velocity reaches the maximum level. When examining the contours, it is evident that this velocity value corresponds to approximately 0.6 m s^{-1} for a mass flow rate of 0.011 kg s^{-1}.

Streamlines are important for understanding the flow field and its characteristics. Additionally, the movement of the fluid between the inlet and outlet regions and its velocity values are seen. The heat transfer is affected negatively at

**Fig. 15** Temperature contours of the water for the cases with 2 TE modules
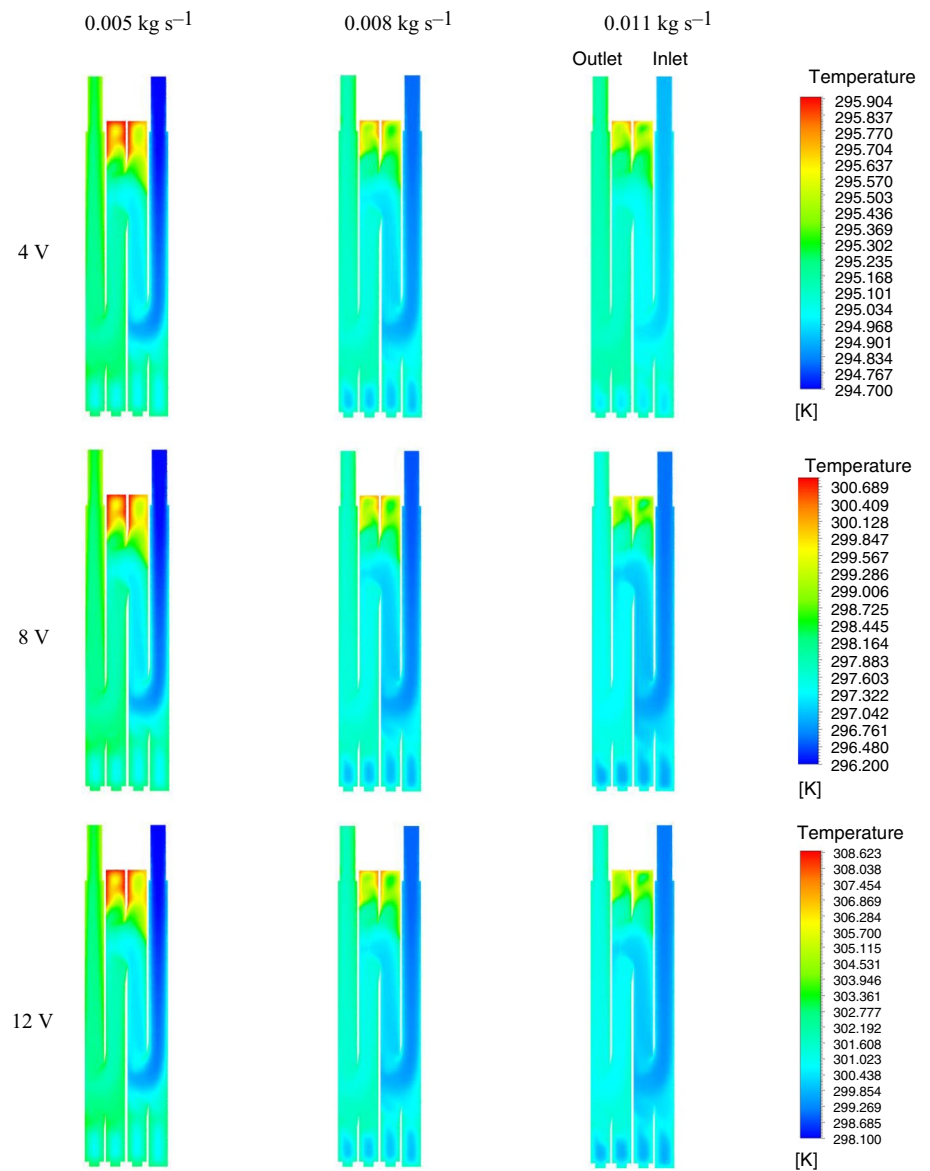
the recirculation zones where fluid is trapped. Because their temperature increases in these regions due to the heat flux, which they are exposed, they cannot get out of the heat sink and prevent cold liquids reaching to these regions.

In Fig. 14, the temperature distribution of the water in the liquid-cooling heat sink is presented for the case with a single TE module. As can be seen from the contours, the hottest water areas for all mass flow rates occur around the outlet area and bottom of the heat sink. Since there are recirculation zones at the bottom of the heat sink, the temperature increased and the heat transfer decreased in these regions.

In Fig. 15, the temperature contours of the fluid are given at different flow rates and voltages for in the case of 2 TE modules. Since the second TE module is placed on the region 1 shown in Fig. 2, it is seen that the temperature of the cooling water reaches the highest values in this region. It is also seen that the difference between the water inlet and outlet temperatures decreases as the flow rate increases.

The temperature contours of the fluid obtained in the numerical solution performed for the case with 3 TE modules are presented in Fig. 16. In the mentioned case, the usage of 3 modules have increased both the amount of heat

Fig. 16 Temperature contours
of the water for the cases with 3
TE modules
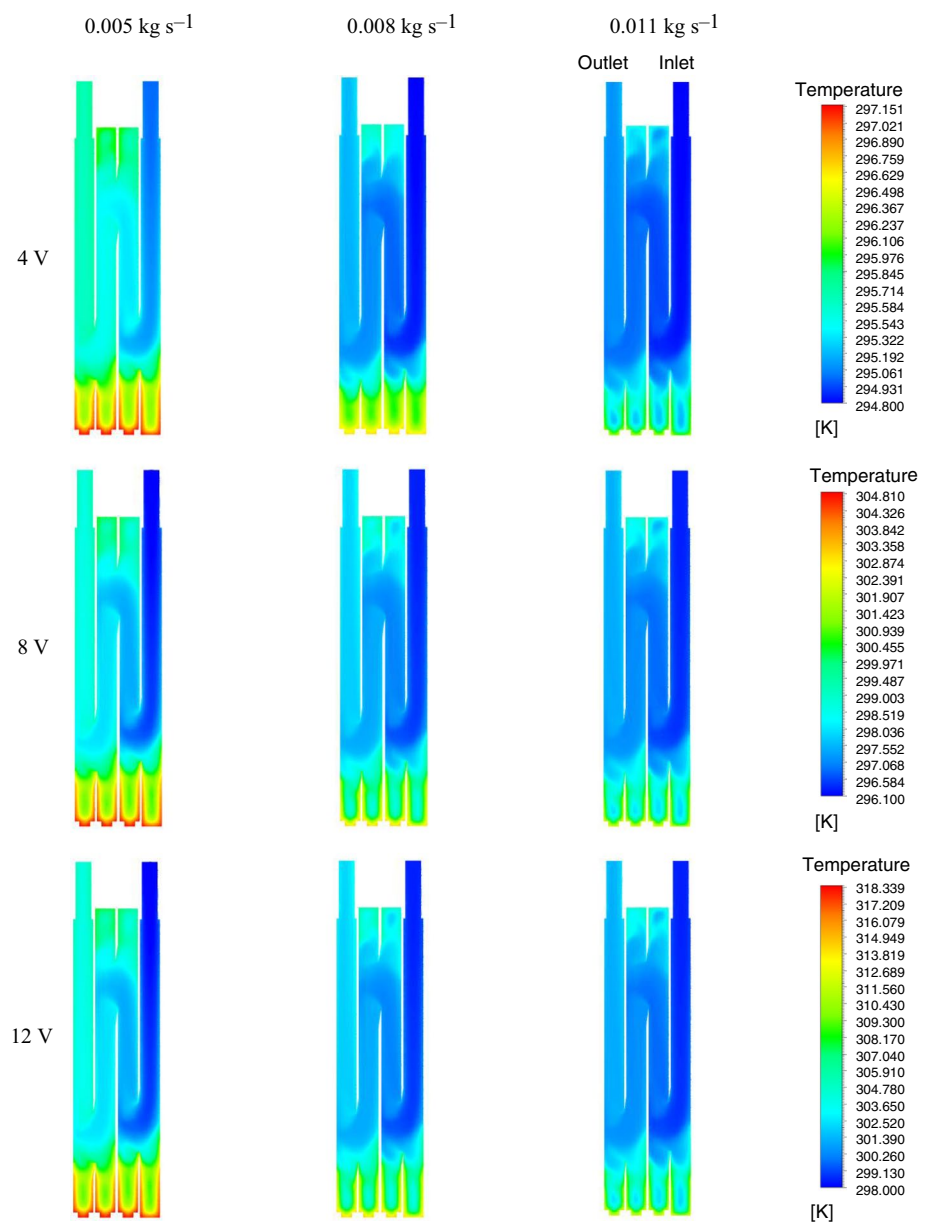
energy transferred to the cooling water and the temperature difference in the inlet and outlet compared to the other two conditions. In addition, since the increased operating voltage caused more heating on the hot surface of the TE module, it caused the cooling water to reach higher outlet temperatures, for all TE modes as expected.

In Fig. 17, the temperature contours of the liquid-cooling heat sink are given for operating conditions with a single TE module. Since there is heat transfer from the TE module to the heat sink, the middle region of the heat sink, where the TE module is placed, seems to have a higher temperature than the other regions. It has been determined that as the mass flow rate of the heat transfer fluid increases, the heat sink temperature goes down, and heat transfer rate improves.

The temperature contours of the heat sink in the system using 2 TE modules are shown in Fig. 18. Since the heat flux is applied to the beginning and middle of the heat sink,

Fig. 17 Temperature contours of the heat sink for the cases with 1 TE module
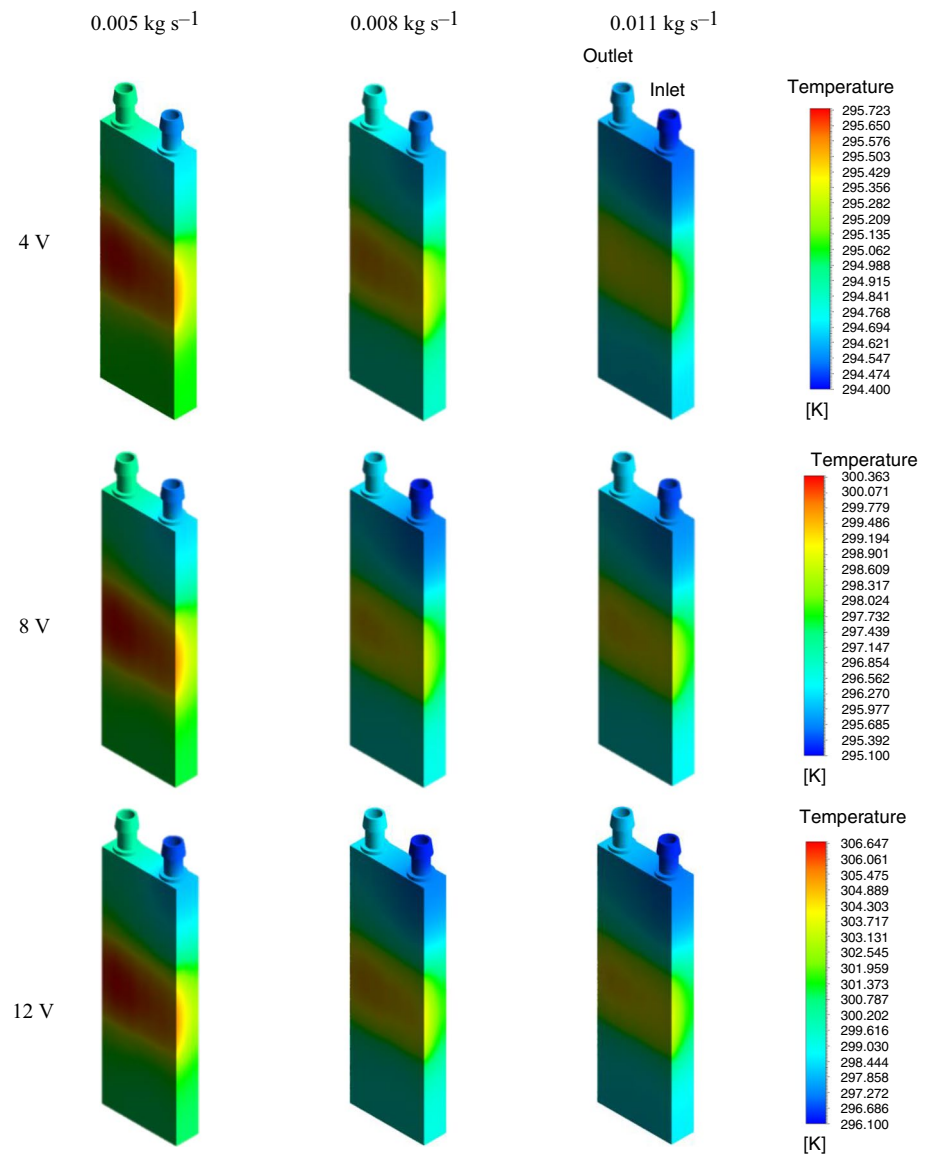
the temperature of these regions has taken higher values than the other regions. The temperature of the water entering the heat sink at low temperature increased as a result of heat absorption from the system. For this reason, the cooling performance near the outlet area of the heat sink was lower than in other areas. As displayed in the figure, at the lowest mass flow rate (0.005 kg s^{-1}), the accumulated thermal energy could not dissipate rapidly due to the low fluid flow velocity. Consequently, the fluid temperature rises, and the block exchanger reaches higher temperatures. As the mass

flow rate rises to higher levels of 0.008 and 0.011 kg s^{-1}, fluid velocity increases, and thermal energy is extracted rapidly from the domain and the block exchanger exhibits lower temperatures along with the heat transfer fluid.

In Fig. 19, heat sink temperature contours for the case with 3 TE modules are shown. Since the fluid circulation at the bottom of the heat sink cannot be fully ensured, the temperature takes the highest values in these regions. As the

Fig. 18 Temperature contours of the heat sink for the cases with 2 TE modules
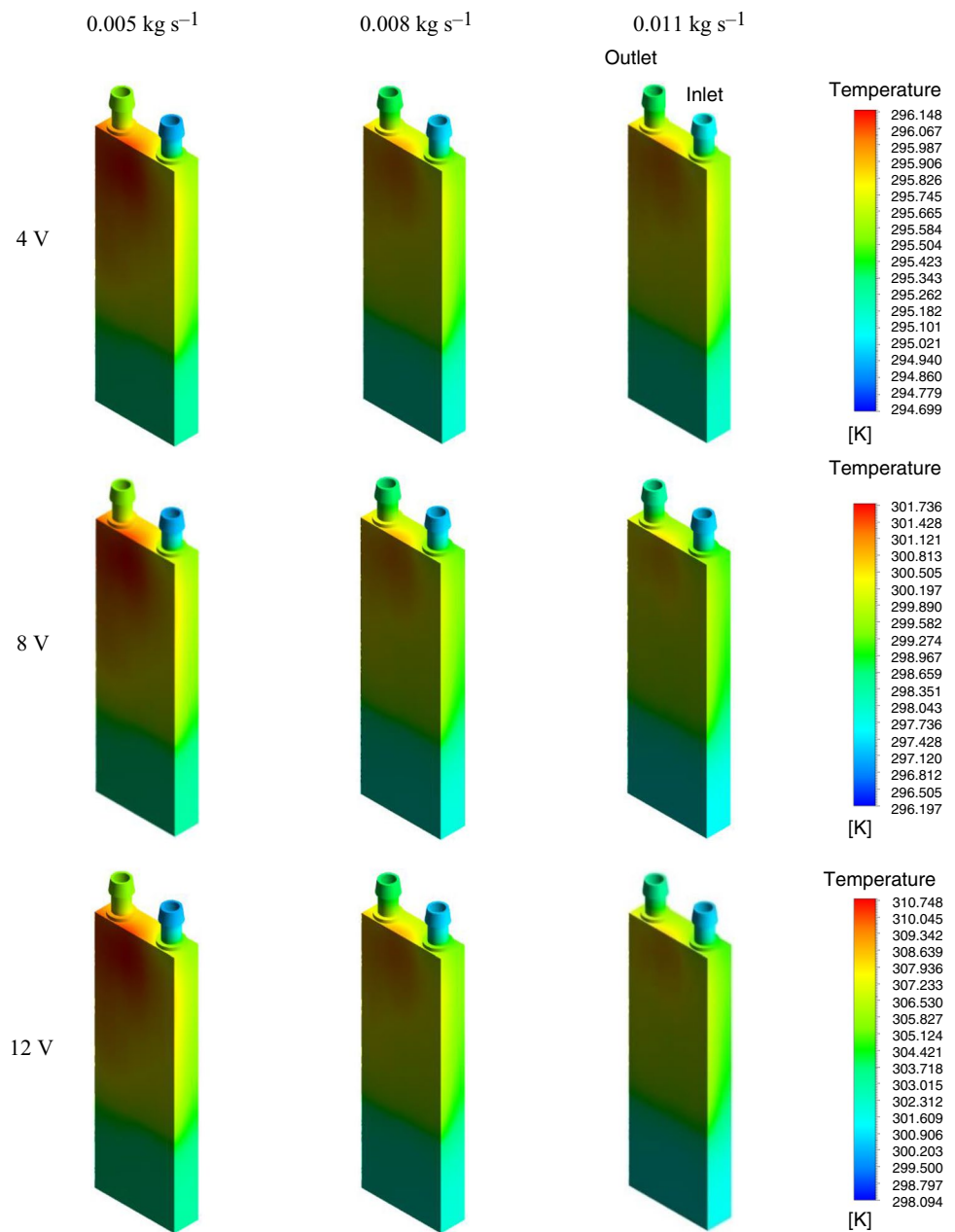

voltage increases, the temperature of the heat sink, which is exposed to a higher heat flux, also increases. It is also seen that a more effective cooling occurs with an increase in the flow rate.

In Fig. 20, temperature distributions of water and heat sink at constant voltage and mass flow rate are given according to the numbers of TE module. As the number of TE modules increases, the amount of heat energy transferred to the water increases, so the inlet and outlet temperature difference of the water increases. Also, the temperature of the regions where the TE modules are located is higher, because they are directly exposed to the heat flux.

Fig. 19 Temperature contours of the heat sink for the cases with 3 TE modules
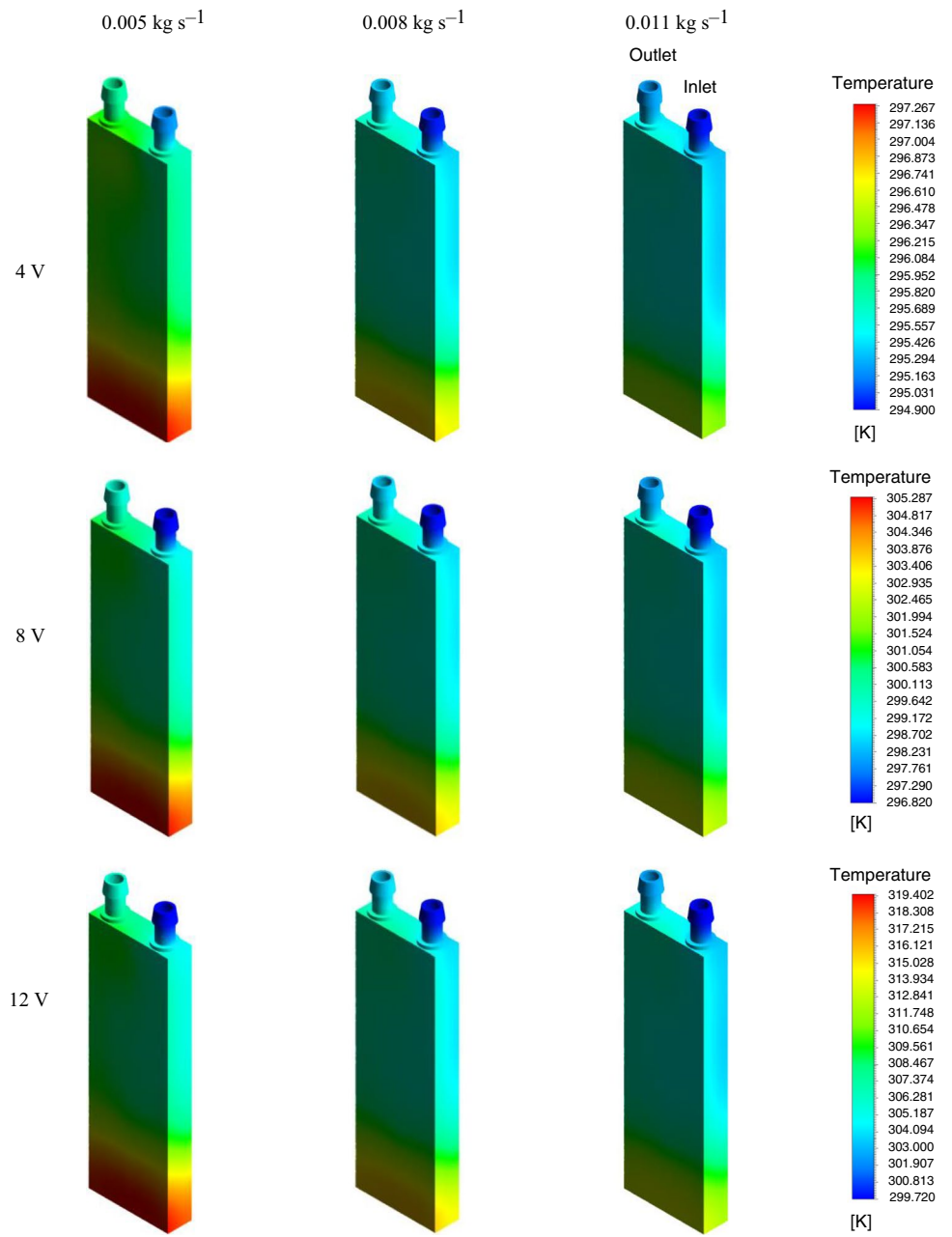
Fig. 20 Temperature distribution of water and heat sink with numbers of TE Module at 0.005 kg s^{-1} mass flow rate and 12 V voltage applied

1 TE module   2 TE module   3 TE module
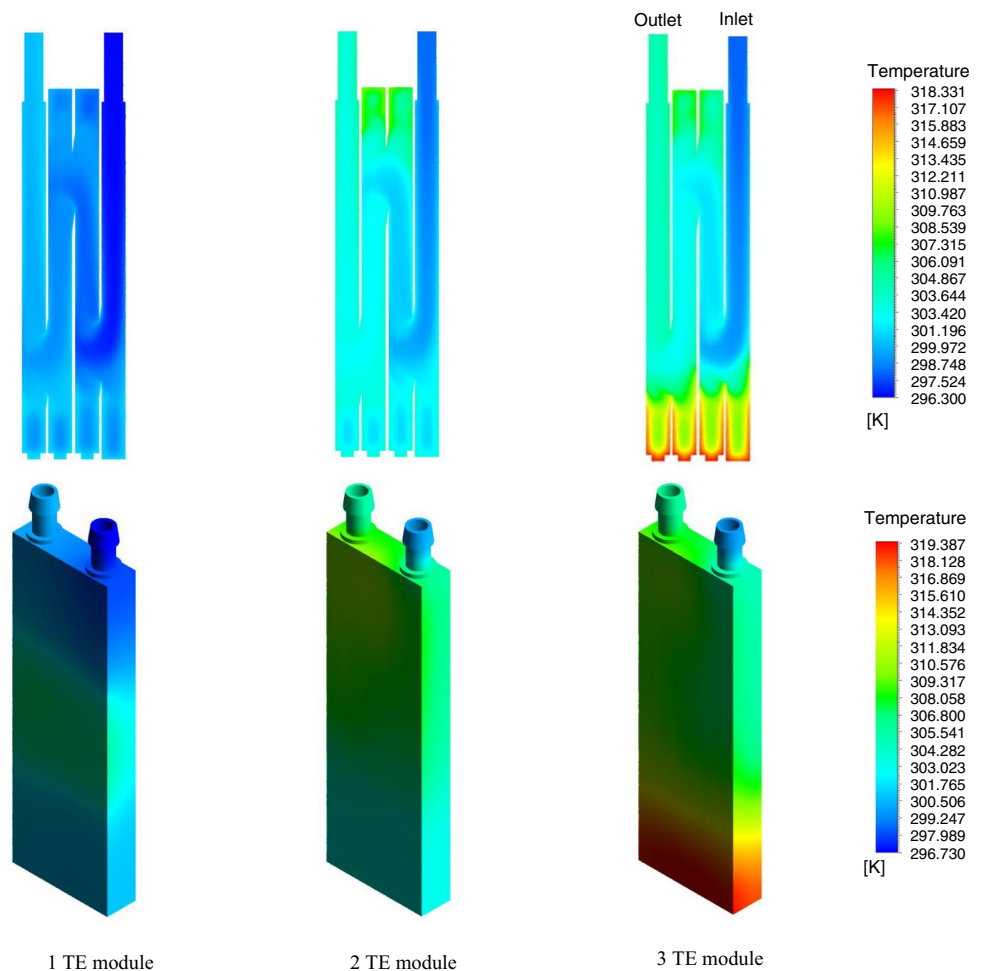
Conclusions

In TE coolers, how the TE module will be cooled is as important as the heat drawn from the cooling chamber. In order to obtain high performance from TE modules, the hot surface of TE should be cooled effectively, which is possible with the correct selection of the operating conditions of the TEs. In this context, the effects of TE number, operating voltage, water flow rate and using triple block heat exchanger on the cooling chamber temperature and cooling performance were investigated. Additionally, detailed numerical analyses were made for a water-cooled triple type heat exchanger used in the cooling of the TE module and the effect of this heat exchanger on the TE cooler performance was also evaluated. From the comprehensive CFD analyses, the temperature distribution of the heat transfer fluid and the heat exchanger surface were explored. Furthermore, CFD results visualized the fluid dynamics within the block heat exchanger using streamlines and velocity contours, providing insights that are typically unattainable through experimental methods.

Moreover, the issue of heat losses, which is often neglected in the literature, was also examined and discussed within the scope of the study. The effect of double foam thermal insulation on the cooling chamber temperature was also discussed. It was found that the cooling load increased with the increase in the number of thermoelectric modules in the designed cooling system. This will be valid as long as the TE modules can be cooled effectively. In addition, the total energy consumption of the TE cooler increases with the increasing number of modules. As a result of increased energy consumption, a significant decrease was observed in the COP value of the cooling system. It was observed that when the supply voltage is increased, a significant increase in the cooling load was obtained at high water flow rates, where effective cooling can be achieved. On the other hand, the increase in supply voltage at low flow rates caused insufficient cooling of the TE module. As a result, the TE cooler was negatively affected in terms of the cooling load. At 0.011 kg s^{-1} mass flow rate and 12 V voltage conditions, when the number of TE modules is increased from 1 to 3 in the TE cooler, a maximum

increase of 35% in cooling load is obtained. This increase can reach 80% by increasing the supply voltage. According to insulation tests, it was observed that a significant amount of heat loss occurred in the cooling chamber. In order to minimize these losses, the chamber insulation was doubled, resulting in an additional 2 °C temperature drop in cooling chamber. As a result of the numerical analysis, the presence of recirculation zones that probably prevent effective cooling and inappropriate channel contact zones in the water-cooled triple block heat exchanger was determined. The thermal performance of the TE cooler can be taken a step further if these problems can be eliminated in the design of the water-cooled block. In future research endeavors, a deeper exploration of the optimal operational conditions of the thermoelectric cooling system, including the number of thermoelectric modules, voltage levels, and flow rates, is imperative to maximize its efficiency. Additionally, there is a pressing need to enhance thermal insulation strategies, examining various insulation materials and configurations to reduce heat losses and consequently improve the system's overall performance. Alternative materials and innovative design approaches should also be investigated to potentially yield more cost-effective and energy-efficient systems. Moreover, a focus on sustainability and energy efficiency will be pivotal in evaluating the contributions of thermoelectric cooling technology to environmental conservation and sustainable energy practices.

Declarations

Conflict of interest The authors declare that they have no conflict of interest.

References

1. Mao J, Chen G, Ren Z. Thermoelectric cooling materials. Nat Mater. 2021;20(4):454–61.
2. Enescu D, Virjoghe EO. A review on thermoelectric cooling parameters and performance. Renew Sustain Energy Rev. 2014;38:903–16.
3. Zhao D, Tan G. A review of thermoelectric cooling: materials, modeling and applications. Appl Therm Eng. 2014;66(1–2):15–24.
4. Sahoo RR, Srivastava K. Performance assessment of a new energy harvesting system using thermoelectric generator coupled with solar radiation on hybrid nanofluids. J Therm Anal Calorim. 2022;147(21):12269–84.
5. Dresselhaus MS, Chen G, Tang MY, Yang RG, Lee H, Wang DZ, Ren Z, Fleurial JP, Gogna P. New directions for low-dimensional thermoelectric materials. Adv Mater. 2007;19(8):1043–53.
6. Hand CT, Peuker S. An experimental study of the influence of orientation on water condensation of a thermoelectric cooling heatsink. Heliyon. 2019;5(10):e02752.
7. Al-Shehri S, Saber HH. Experimental investigation of using thermoelectric cooling for computer chips. J King Saud Univ Eng Sci. 2020;32(5):321–9.
8. Putra N, Iskandar FN. Application of nanofluids to a heat pipe liquid-block and the thermoelectric cooling of electronic equipment. Exp Therm Fluid Sci. 2011;35(7):1274–81.
9. Liu D, Zhao FY, Yang HX, Tang GF. Thermoelectric mini cooler coupled with micro thermosiphon for CPU cooling system. Energy. 2015;83:29–36.
10. Liu D, Cai Y, Zhao FY. Optimal design of thermoelectric cooling system integrated heat pipes for electric devices. Energy. 2017;128:403–13.
11. Lyu Y, Siddique ARM, Gadsden SA, Mahmud S. Experimental investigation of thermoelectric cooling for a new battery pack design in a copper holder. Results Eng. 2021;10:100214.
12. Lyu Y, Siddique ARM, Majid SH, Biglarbegian M, Gadsden SA, Mahmud S. Electric vehicle battery thermal management system with thermoelectric cooling. Energy Rep. 2019;5:822–7.
13. Moazzez AF, Najafi G, Ghobadian B, Hoseini SS. Numerical simulation and experimental investigation of air cooling system using thermoelectric cooling system. J Therm Anal Calorim. 2020;139(4):2553–63.
14. Duan M, Sun H, Lin B, Wu Y. Evaluation on the applicability of thermoelectric air cooling systems for buildings with thermoelectric material optimization. Energy. 2021;221:119723.
15. Ismaila KG, Sahin AZ, Yilbas BS, Al-Sharafi A. Thermo-economic optimization of a hybrid photovoltaic and thermoelectric power generator using overall performance index. J Therm Anal Calorim. 2021;144:1815–29.
16. Benghanem M, Al-Mashraqi AA, Daffallah KO. Performance of solar cells using thermoelectric module in hot sites. Renew Energy. 2016;89:51–9.
17. Singh D, Chaubey H, Parvez Y, Monga A, Srivastava S. Performance improvement of solar PV module through hybrid cooling system with thermoelectric coolers and phase change material. Sol Energy. 2022;241:538–52.
18. Cheng TC, Cheng CH, Huang ZZ, Liao GC. Development of an energy-saving module via combination of solar cells and thermoelectric coolers for green building applications. Energy. 2011;36(1):133–40.
19. Wan QS, Su JJ, Huang YY, Wang YP, Liu X. Numerical and experimental investigation on symmetrical cross jet of localized air conditioning system with thermoelectric cooling devices in commercial vehicles. Int J Refrig. 2022;140:29–38.
20. Wan Q, Deng Y, Su C, Wang Y. Optimization of a localized air conditioning system using thermoelectric coolers for commercial vehicles. J Electron Mater. 2017;46(5):2990–8.
21. Yang J, Stabler FR. Automotive applications of thermoelectric materials. J Electron Mater. 2009;38(7):1245.
22. Afshari F, Ceviz MA, Mandev E, Yıldız F. Effect of heat exchanger base thickness and cooling fan on cooling performance of air-to-air thermoelectric refrigerator; experimental and numerical study. Sustain Energy Technol Assess. 2022;52:102178.
23. Abdul-Wahab SA, Elkamel A, Al-Damkhi AM, Is'haq A, Al-Rubai'ey HS, Al-Battashi AK, Al-Tamimi AR, Al-Mamari H, Chutani MU. Design and experimental investigation of portable solar thermoelectric refrigerator. Renew Energy. 2009;34(1):30–4.

24. Manikandan S, Selvam C, Praful PPS, Lamba R, Kaushik SC, Zhao D, Yang R. A novel technique to enhance thermal performance of a thermoelectric cooler using phase-change materials. J Therm Anal Calorim. 2020;140:1003–14.

25. Astrain D, Aranguren P, Martínez A, Rodríguez A, Pérez MG. A comparative study of different heat exchange systems in a thermoelectric refrigerator and their influence on the efficiency. Appl Therm Eng. 2016;103:1289–98.

26. Sarkar A, Mahapatra SK. Role of surface radiation on the functionality of thermoelectric cooler with heat sink. Appl Therm Eng. 2014;69(1–2):39–45.

27. Baldry M, Timchenko V, Menictas C. Optimal design of a natural convection heat sink for small thermoelectric cooling modules. Appl Therm Eng. 2019;160:114062.

28. He B, Chen W, Tan X, Lu S, Zhang J, Li X. Investigation of natural convection characteristics in the molding chamber of a 3-D printer cooled by thermoelectric cooling modules. Int J Mech Sci. 2022;224:107315.

29. He RR, Zhong HY, Cai Y, Liu D, Zhao FY. Theoretical and experimental investigations of thermoelectric refrigeration box used for medical service. Procedia Eng. 2017;205:1215–22.

30. Çağlar A. Optimization of operational conditions for a thermoelectric refrigerator and its performance analysis at optimum conditions. Int J Refrig. 2018;96:70–7.

31. Vian JG, Astrain D. Development of a heat exchanger for the cold side of a thermoelectric module. Appl Therm Eng. 2008;28(11–12):1514–21.

32. Ceviz MA, Afshari F, Muratçobanoğlu B, Ceylan M, Manay E. Computational fluid dynamics simulation and experimental investigation of a thermoelectric system for predicting influence of applied voltage and cooling water on cooling performance. Int J Numer Methods Heat Fluid Flow. 2022;33(1):241–62.

33. Martínez A, Astrain D, Rodríguez A, Pérez G. Reduction in the electric power consumption of a thermoelectric refrigerator by experimental optimization of the temperature controller. J Electron Mater. 2013;42(7):1499–503.

34. Siahmargoi M, Rahbar N, Kargarsharifabad H, Sadati SE, Asadi A. An experimental study on the performance evaluation and thermodynamic modeling of a thermoelectric cooler combined with two heatsinks. Sci Rep. 2019;9(1):1–11.

35. Riffat SB, Omer SA, Ma X. A novel thermoelectric refrigeration system employing heat pipes and a phase change material: an experimental investigation. Renew Energy. 2001;23(2):313–23.

36. Afshari F. Experimental and numerical investigation on thermoelectric coolers for comparing air-to-water to air-to-air refrigerators. J Therm Anal Calorim. 2021;144(3):855–68.

37. Chavan P, Sidhu GK, Alam MS, Kumar M. Mathematical design and performance investigation of evaporator water cooled storage-cum-mobile thermoelectric refrigerator for preservation of fruits and vegetables. J Food Process Eng. 2021;44(8):13770.

38. Cuce E, Guclu T, Cuce PM. Improving thermal performance of thermoelectric coolers (TECs) through a nanofluid driven water to air heat exchanger design: An experimental research. Energy Convers Manag. 2020;214:112893.

39. Gökçek M, Şahin F. Experimental performance investigation of minichannel water cooled-thermoelectric refrigerator. Case Stud Therm Eng. 2017;10:54–62.

40. Vián JG, Astrain D. Development of a thermoelectric refrigerator with two-phase thermosyphons and capillary lift. Appl Therm Eng. 2009;29(10):1935–40.

41. Min G, Rowe DM. Experimental evaluation of prototype thermoelectric domestic-refrigerators. Appl Energy. 2006;83(2):133–52.

42. Rahman SMA, Hachicha AA, Ghenai C, Saidur R, Said Z. Performance and life cycle analysis of a novel portable solar thermoelectric refrigerator. Case Stud Therm Eng. 2020;19:100599.

43. Abderezzak B, Dreepaul RK, Busawon K, Chabane D. Experimental characterization of a novel configuration of thermoelectric refrigerator with integrated finned heat pipes. Int J Refrig. 2021;131:157–67.

44. Mirmanto M, Syahrul S, Wirdan Y. Experimental performances of a thermoelectric cooler box with thermoelectric position variations. Eng Sci Technol Int J. 2019;22(1):177–84.

45. Ohara B, Sitar R, Soares J, Novisoff P, Nunez-Perez A, Lee H. Optimization strategies for a portable thermoelectric vaccine refrigeration system in developing communities. J Electron Mater. 2015;44(6):1614–26.

46. Jugsujinda S, Vora-ud A, Seetawan T. Analyzing of thermoelectric refrigerator performance. Procedia Eng. 2011;8:154–9.

47. Tamami F, Doyan A, Ayub S, Hudha LS. Designing and constructing mini refrigerator with thermoelectric module. J Phys Conf Ser. 2022;2165:012032.

48. Hermes CJ, Barbosa JR. Thermodynamic comparison of Peltier, Stirling, and vapor compression portable coolers. Appl Energy. 2012;91(1):51–8.

49. Park H, Lee J, Lim J, Cho H, Kim J. Optimal operating strategy of ash deposit removal system to maximize boiler efficiency using CFD and a thermal transfer efficiency model. J Ind Eng Chem. 2022;110:301–17.

50. Afshari F, Mandev E, Rahimpour S, Muratçobanoğlu B, Şahin B, Manay E, Teimuri-Mofrad R. Experimental and numerical study on air-to-nanofluid thermoelectric cooling system using novel surface-modified Fe_3O_4 nanoparticles. Microfluid Nanofluid. 2023;27(4):26.

51. Afshari F, Zavaragh HG, Sahin B, Grifoni RC, Corvaro F, Marchetti B, Polonara F. On numerical methods; optimization of CFD solution to evaluate fluid flow around a sample object at low Re numbers. Math Comput Simul. 2018;152:51–68.

52. Afshari F, Tuncer AD, Sözen A, Variyenli HI, Khanlari A, Gürbüz EY. A comprehensive survey on utilization of hybrid nanofluid in plate heat exchanger with various number of plates. Int J Numer Methods Heat Fluid Flow. 2021;32(1):241–64.

53. Güngör A, Khanlari A, Sözen A, Variyenli HI. Numerical and experimental study on thermal performance of a novel shell and helically coiled tube heat exchanger design with integrated rings and discs. Int J Therm Sci. 2022;182:107781.